Title
Effects of lattice geometry on the dynamic properties of dipolar-coupled magnetic nanodisk arrays

Journal
Physical Review B, 99(6)

ISSN
2469-9950

Authors
Slöetjes, Sam D
Digernes, Einar
Klewe, Christoph
et al.

Publication Date
2019-02-01

DOI
10.1103/physrevb.99.064418

Peer reviewed

Effects of lattice geometry on the dynamic properties of dipolar-coupled magnetic nanodisk arrays

Sam D. Slöetjes,[1,2,*] Einar Digernes,[1] Christoph Klewe,[2] Padraic Shafer,[2] Q. Li,[3] M. Yang,[3] Z. Q. Qiu,[3] Alpha T. N'Diaye,[2] Elke Arenholz,[2] Erik Folven,[1] and Jostein K. Grepstad[1]

[1]*Department of Electronic Systems, NTNU, NO-7491, Trondheim, Norway*

[2]*Advanced Light Source, LBNL, Berkeley, California 94720, USA*

[3]*Department of Physics, UC Berkeley, Berkeley, California 94720, USA*

We have studied the impact of lattice geometry on the dynamic properties of close-spaced arrays of circular nanomagnets, also known as magnonic crystals. To this end, we prepared 2D nanomagnet arrays with both square and hexagonal lattice symmetries (300-nm disk diameter, 400-nm center-to-center distance) and performed broadband ferromagnetic resonance (FMR) measurements. Micromagnetic simulations were used to interpret distinct features of the measured resonance spectra. The FMR bias field was applied along two distinct principal directions for each lattice, and a sample with well-separated, decoupled disks was measured for reference. We found that the interdisk dipolar coupling has a strong impact on the FMR for these 2D magnonic crystals. Distinctly different oscillation modes were found for the individual nanomagnets, dependent on lattice symmetry and direction of the bias field. Moreover, we find that spectral peak splitting from excitation of edge and center modes, as well as the damping, depends on the lattice symmetry and the orientation of the bias field. These findings demonstrate that lattice geometry has a strong influence on the excited spin-wave spectrum and is a relevant design parameter for spintronic devices.

I. INTRODUCTION

Magnonic crystals are metamaterials in which the magnetic properties vary periodically [1]. These analogs to photonic crystals offer unprecedented tunability of the magnetodynamics [2–4]. A special application of such systems is generation of highly tunable microwaves from a nanoscale source [4]. Examples of magnonic crystals are magnetic thin films with nonmagnetic holes placed in a periodic fashion [5,6] or dipolar-coupled ferromagnetic nanodots [7], as discussed in this paper. The dynamics of single isolated magnetic dots have been investigated extensively [8–11], whereas studies of closely spaced, dipolar-coupled systems are few [12–14]. The dynamic properties of magnonic crystals are still poorly understood due to the high complexity of periodic dipolar-coupled systems [14]. Here, we present ferromagnetic resonance (FMR) studies of the spectral response of magnonic crystals, dependent on their symmetry and the bias-field direction.

II. METHODS

The magnonic crystal samples were made from 15-nm permalloy (Py) films, deposited on a silicon substrate and capped with a 2-nm aluminum oxide layer to serve as the oxidation barrier. Using electron-beam lithography, the films were patterned into arrays of disks with diameter $d = 300$ nm and a center-to-center distance of 400 nm, shown in Figs. 1(a) and 1(b). This results in an edge-to-edge spacing of 100 nm, i.e., less than the disk diameter, and ensures sufficient dipole-dipole interaction to impact the dynamic properties of the arrays. The patterned area on each sample was 3×3 mm^2 in order to ensure sufficient absorbed power in the FMR experiment.

We performed broadband FMR measurements by acquiring FMR spectra at a constant microwave frequency while sweeping the external field, $\mu_0 H_0$, from 150 to 0 mT. The initial field of 150 mT ensures magnetic saturation of the disks for the FMR experiments. In this setup, the sample is placed face down on a coplanar waveguide, where the microwave radiation is applied at frequencies from 3 to 12 GHz in increments of 1 GHz. The field derivative of the FMR absorption intensity was measured using an rf diode and using a lock-in amplifier at an ac modulation field of 133 Hz. In order to probe the anisotropy originating from intermagnet dipolar coupling, we applied the field along two high-symmetry lattice directions for each nanodisk array. For the square lattice, we applied the field $\mu_0 H_0$ in the in-plane [10] and [11] directions, and for the hexagonal lattice the field was applied in the $[1\bar{2}]$ and $[\bar{1}0]$ directions; cf. Figs. 1(a) and 1(b). In the hexagonal lattice, these directions correspond to a direction of nearest neighbors and a direction between nearest neighbors, respectively. Hysteresis loops measured using x-ray magnetic circular dichroism spectroscopy at beamline 6.3.1 at the Advanced Light Source showed a remanent magnetization close to saturation, confirming that the individual magnets remain in a monodomain state throughout this measurement range. In order to determine the spectral linewidths and resonance peak positions, we fitted the resulting spectra with a superposition of derivative and double-derivative Lorentzians [15].

*Corresponding author: sam.sloetjes@ntnu.no

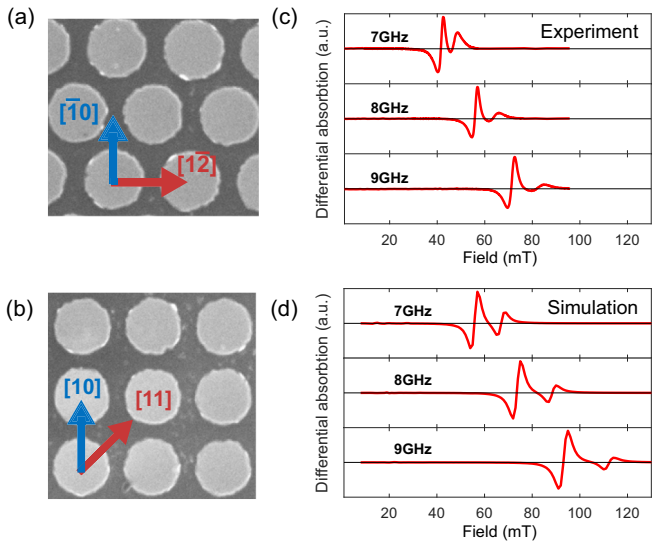

FIG. 1. (a) SEM image of the magnonic crystal with (a) hexagonal symmetry and (b) square symmetry. The disks are 300 nm in diameter with 100-nm separation. The lattice principal axes are indicated with red and blue arrows. (c) Measured and (d) simulated FMR absorption spectra for frequencies of 7–9 GHz for the square array, with the applied field oriented in the [11] direction.

For the micromagnetic simulations, we used the software package MUMAX3, which solves the Landau-Lifshitz-Gilbert equation numerically for a given geometry [16]. The material parameters used to describe the magnetic properties of the nanomagnets are standard values for Py, i.e., exchange stiffness $A_{\mathrm{ex}} = 10\,\mathrm{pJ/m}$, saturation magnetization $M_{\mathrm{S}} = 800\,\mathrm{kA/m}$, and a crystalline anisotropy of $0\,\mathrm{J/m^3}$. The damping parameter was set to $\alpha = 0.01$, a typical value for patterned Py elements. The simulation cell size was optimized for mesh independence, to avoid anisotropies resulting from projection of the circular nanodisks onto a square grid. However, the cells were large enough so that computation times were within reasonable bounds. The chosen cells had in-plane dimensions of 2.5 nm×2.5 nm for the hexagonal lattice and 1.5 nm×1.5 nm for the square lattice, both smaller than the magnetostatic exchange length, $l_{\mathrm{S}} = \sqrt{2A_{\mathrm{ex}}/\mu_0 M_{\mathrm{S}}^2} = 4.98$ nm. The simulated FMR spectra were obtained by exciting the magnetic moments with an in-plane field pulse in the direction perpendicular to H_0. The frequency spectra of the resulting oscillations are found by Fourier transformation, using a procedure known as the "ringdown method" [17,18]. In order to obtain the full frequency spectra, this procedure is repeated for values of the field $\mu_0 H_0$ from 1 to 150 mT in steps of 1 mT. Magnetic nanodisks typically feature both edge and center modes [8], i.e., spatially inhomogeneous oscillations. Thus, the spatial distribution of their amplitude is of interest. By applying the ringdown method to every grid point $\mathbf{m}(x_{\mathrm{n}}, y_{\mathrm{m}}, t)$ to compute Fourier transforms $\tilde{\mathbf{m}}(x_{\mathrm{n}}, y_{\mathrm{m}}, f)$, spatial amplitude and phase maps of the nanodisk oscillations were obtained, for applied bias fields $\mu_0 H_0$ from 20 to 140 mT, in increments of 20 mT.

III. RESULTS AND DISCUSSION

Figures 1(c) and 1(d) compare experimental and simulated (derivative) FMR absorption spectra for the square lattice, with H_0 pointing in the [11] direction and excitation frequencies from 7 to 9 GHz. In this range of frequencies the resonance is split into two separate peaks, centered at different values of $\mu_0 H_0$. The low-field peak retains a substantial amplitude throughout the frequency range, whereas the high-field peak broadens and rapidly attenuates with increasing frequency. The simulated spectra show a similar splitting of the ferromagnetic absorption resonance around 7 GHz, and excellent agreement between simulation and experiment is found. We note there is an offset in peak position H_{FMR} between the simulated and experimental spectra, most likely due to the measurements being carried out at finite temperature ($T = 295$ K).

The spectra were fitted with superpositions of first- and second-derivative Lorentzian functions [15,19]:

$$\frac{dI_{\mathrm{FMR}}}{dH_0} \propto \cos(\epsilon)\frac{2(H_0 - H_{\mathrm{FMR}})\Delta H_{\mathrm{HWHM}}}{\left[\Delta H_{\mathrm{HWHM}}^2 + (H_0 - H_{\mathrm{FMR}})^2\right]^2} + \sin(\epsilon)\frac{\left[\Delta H_{\mathrm{HWHM}}^2 - (H_0 - H_{\mathrm{FMR}})^2\right]}{\left[\Delta H_{\mathrm{HWHM}}^2 + (H_0 - H_{\mathrm{FMR}})^2\right]^2}.$$

Here, H_{FMR} is the peak position, ΔH_{HWHM} is the linewidth defined as the half width at half-maximum (HWHM), and ϵ is the mixing angle between the symmetric and the antisymmetric term. We employed a least-squares fitting method to derive these fitting parameters. The resonance frequencies were subsequently plotted versus peak position H_{FMR}, following the Kittel curve, which can be fitted using the Kittel equation [20]. Measured and simulated Kittel curves for an array of magnetically uncoupled nanodisks (300-nm disk diameter, 800-nm center-to-center distance) are shown in Fig. 2. The Kittel curves for the square lattice, with the bias field H_0 applied along the [10] and [11] directions, are shown in Figs. 3(a) and 3(b), respectively, and results for the hexagonal lattice are shown in Figs. 4(a) and 4(b). The Kittel curves for a single disk and for the square lattice with H_0 oriented in the [10] direction show only one prominent branch. With H_0 oriented in the [11] direction, two branches are obtained [cf. Fig. 4(b)]. For the hexagonal lattice, the Kittel curves with H_0 oriented along either the $[1\bar{2}]$ or $[\bar{1}0]$ directions split into two branches. This splitting occurs at a higher bias field than for the square lattice with H_0 oriented in the [11] direction.

In all cases, the simulated FMR spectra accurately reproduce the spectral features of the experimental data, such as the mode splitting. The corresponding spin-wave amplitude maps for the individual magnets are shown in the insets of Figs. 3 and 4 for the square and hexagonal lattice, respectively. The FMR spectra for the isolated disk and the square lattice with H_0 in the [10] direction are nearly identical, differing only by a small offset in resonance frequency. For these systems, the resonances correspond chiefly to center modes throughout the entire frequency range (3–12 GHz), as can be seen from the insets in Fig. 3. A notable exception is the oscillation mode at an applied field of $\mu_0 H_0 = 60$ mT, which shows a splitting in two spatial maxima rather than a single maximum.

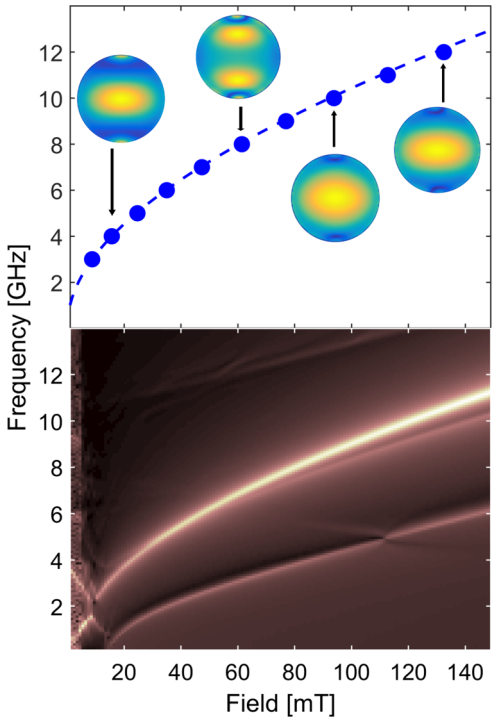

FIG. 2. Upper graph shows the measured Kittel curve for a single disk. Insets show amplitude maps at fields of 20, 60, 100, and 140 mT, as determined by simulations. Lower graph shows corresponding contour plots for simulated absorption spectra. The noise at fields of $\mu_0 H < 5$ mT is a result of some nanomagnets in the simulations having a flux-closure ground state.

For H_0 oriented in the [11] direction, we observe a much different resonance behavior. Here, the principal resonance splits into two branches for a field of approximately 40 mT [cf. Fig. 3(b)]. From simulations, we find that the resonance at low fields arises from a mode with maximal amplitude localized near the edges of the nanodisks, i.e., "edge modes" [cf. insets of Fig. 3(b)]. The high-field part of the Kittel curve features a high- and a low-frequency branch, corresponding to a center mode and an edge mode, respectively. The amplitude maps show that the high-field mode is not a pure edge mode, i.e., there is a finite but small oscillation amplitude for the magnetization throughout the disk. This oscillation is a standing wave, with a wavelength of approximately the diameter of the magnetic disk.

We find a similar behavior for the hexagonal lattice, where the main resonance feature splits into two peaks at an applied field of approximately 60 mT. The resonances beyond this bias field also feature a low-frequency edge mode and a high-frequency center mode, as can be seen in Fig. 4. However, in contrast to the square lattice with the field applied along the [11] direction, the resonance is a center mode in the low-field range (i.e., for $\mu_0 H_0 \leqslant 60$ mT). The two applied field directions in the hexagonal lattice show little difference in the measured and simulated spectra (cf. Fig. 5), suggesting negligible magnetic anisotropy for the hexagonal lattice.

Additional resonances can be observed in the simulated FMR data, such as the branch at approximately half the frequency of the main mode, cf. Figs. 2–4. From the simulated amplitude maps, we find that this resonance corresponds to a pure edge mode (i.e., zero amplitude at the center of the disk). This mode does not show up in the experimental FMR spectra,

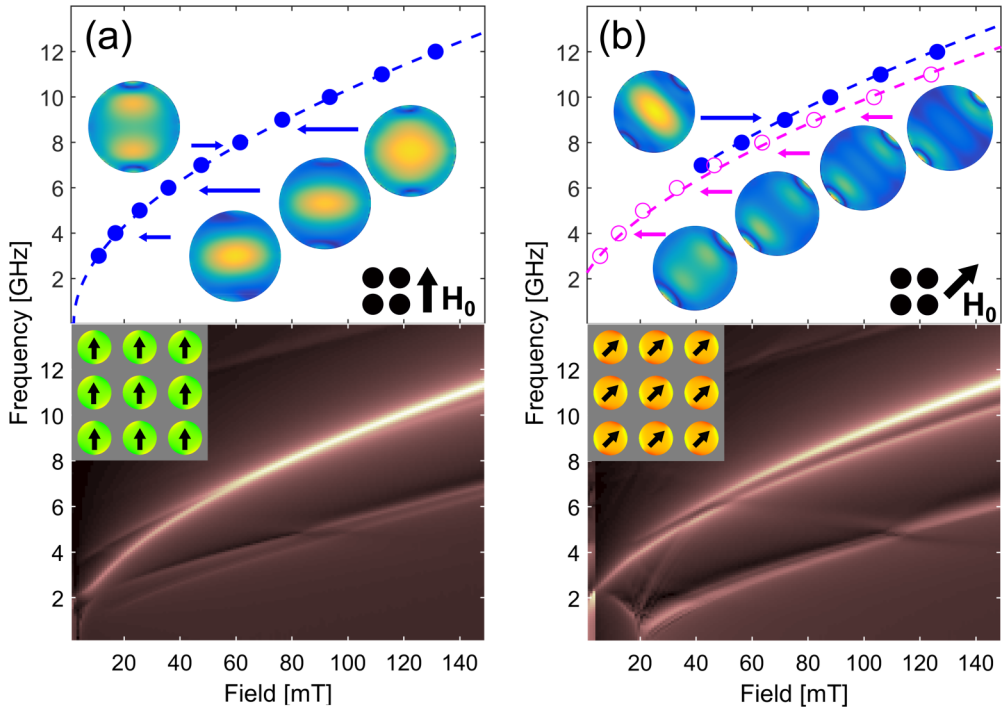

FIG. 3. Upper graphs show measured Kittel curves for the square lattice, with the field in the [10] direction (a) and the [11] direction (b). Blue solid dots and pink open dots represent center- and edge modes, respectively; insets show amplitude maps for applied fields of 20, 40, 60, and 80 mT. Lower graphs show corresponding contour plots for simulated absorption spectra, with insets showing magnetization directions.

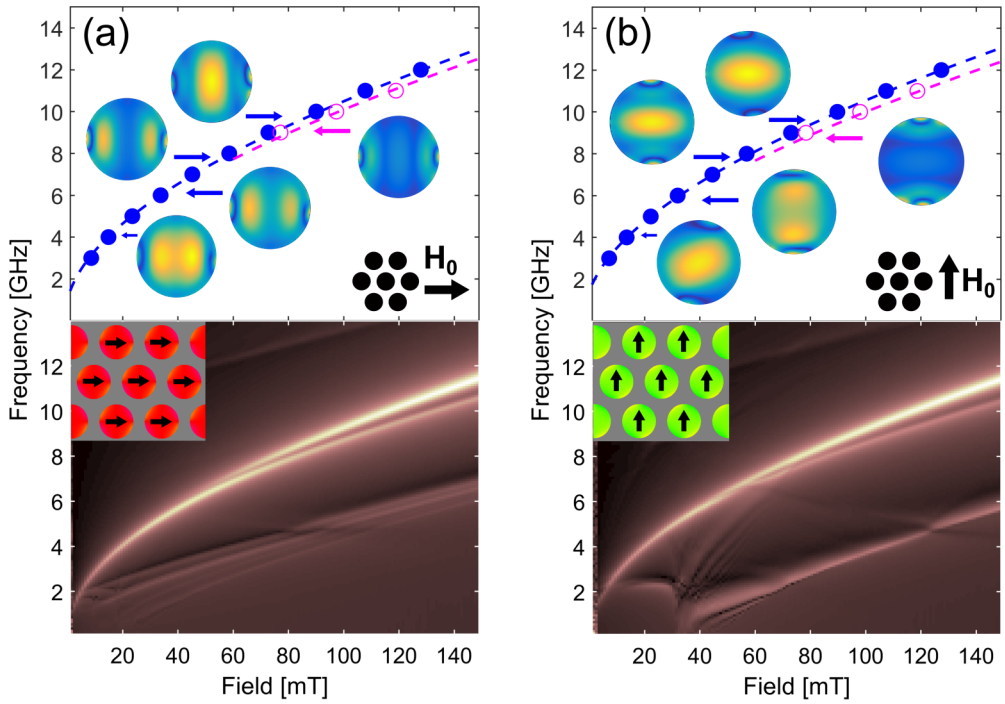

FIG. 4. Upper graphs show measured Kittel curves for the hexagonal lattice, with the field in the [1$\bar{2}$] direction (a) and the [$\bar{1}$0] direction (b). Insets show amplitude maps for applied fields of 20, 40, 60, and 80 mT. Lower graphs show corresponding contour plots for simulated absorption spectra, with insets showing magnetization directions.

most likely because it absorbs too little energy to be detected by our FMR setup.

For the center-mode oscillations of the nanodisk magnetization, we can fit the Kittel equation for an ellipsoid [8,20]:

$$f = \frac{\gamma}{2\pi}\sqrt{\mu_0 H_0 + \mu_0 H_a + \mu_0 M_S(N_y - N_x)} \times \sqrt{\mu_0 H_0 + \mu_0 H_a + \mu_0 M_S(N_z - N_x)}.$$

Here, $N_{x,y,z}$ represent the demagnetization factors, H_a is the anisotropy field, M_S is the saturation magnetization, μ_0 is the permeability of free space, and γ is the gyromagnetic ratio. In our case, the disks are lying in the xy plane, and the bias field, H_0, is applied in the x direction. Because of the circular symmetry, we have $N_y = N_x$ so that the term $N_y - N_x$ vanishes, and we are left with

$$f = \frac{\gamma}{2\pi}\sqrt{\mu_0 H_0 + \mu_0 H_a} \times \sqrt{\mu_0 H_0 + \mu_0 H_a + \mu_0 M_S(N_z - N_x)}. \quad (1)$$

As the saturation magnetization for a blanket Py film has been determined by vibrating sample magnetometry, the demagnetization factor difference $(N_z - N_x)$ and the anisotropy field $\mu_0 H_a$ are free fitting parameters.

For the square-lattice edge mode measured with the bias field in the [11] direction, we take into account standing spin waves in the fitting procedure. The dispersion relation for magnetostatic spin waves (i.e., spin waves with a large wavelength, virtually unaffected by the exchange energy) is given by [9,21,22]

$$f(k) = \frac{\gamma}{2\pi}\sqrt{\mu_0 H_0} \times \sqrt{\mu_0 H_0 + \mu_0 M_S \cdot F_D(k)} \quad (2)$$

Here, $F_D(k)$ is a correction factor which arises from the dipole-dipole coupling between the spins, and k is the wave vector of the spin wave. Combining Eqs. (1) and (2), we obtain

$$f(k) = \frac{\gamma}{2\pi}\sqrt{\mu_0 H_0 + \mu_0 H_a} \times \sqrt{\mu_0 H_0 + \mu_0 H_a + \mu_0 M_S(N_z - N_x) \cdot F_D(k)}. \quad (4)$$

We fitted the Kittel equation for the center mode [Eq. (1)] to the relevant branch in Fig. 3(b) to obtain values for $(N_z - N_x)$ and H_a. For the square lattice, this fitting resulted in anisotropy fields of $\mu_0 H_a = 5$ mT and $\mu_0 H_a = -2$ mT for the field aligned along the [11] and [10] directions, respectively. Fitted values for the hexagonal lattice were $\mu_0 H_a = 1$ mT and $\mu_0 H_a = 2$ mT for the field aligned along the [1$\bar{2}$] or [$\bar{1}$0] directions, respectively. This leaves $F_D(k)$ as the free fitting parameter in Eq. (4) for the edge mode. The best fit was found for $F_D(k) = 0.9$. Taking $F_D(k)$ to have the form valid for a blanket film, i.e., $F_D(k) = (1 - e^{-kd})/kd$, where d is the film thickness; the fitted wave vector k corresponds to a spin-wave wavelength of $\lambda_{dip} \approx 350$ nm, which is approximately the disk diameter. This result is in close agreement with the micromagnetic simulations.

The center-mode branches in Figs. 4(a) and 4(b) have a difference in anisotropy field $\mu_0 H_a$ of 1 mT, which is within the error margin of ± 1 mT. This finding suggests that the hexagonal lattice shows little to no anisotropy in the FMR response, which corresponds well to theoretical predictions that a hexagonal lattice of dipolar-coupled disks has a continuous degeneracy with respect to the in-plane magnetization direction [23]. For the hexagonal lattice, the only distinct difference between the [1$\bar{2}$] and the [$\bar{1}$0] orientations of H_0 is

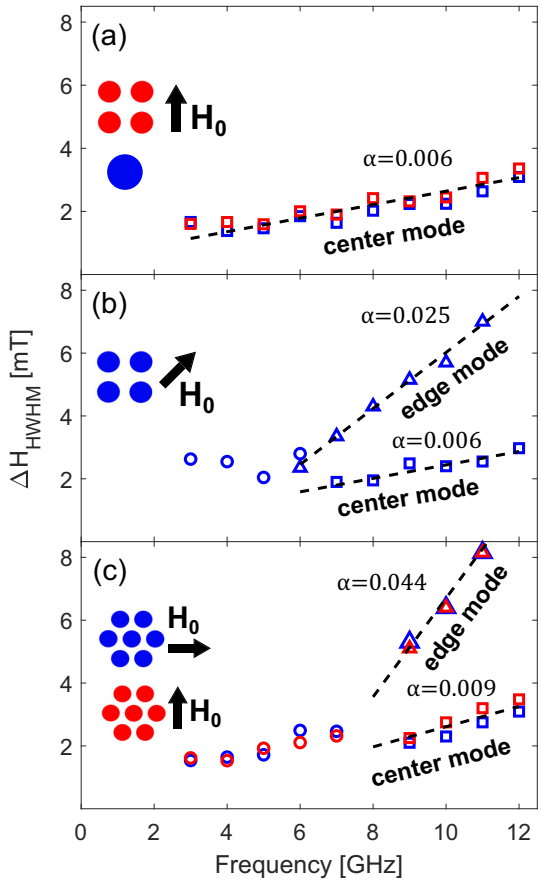

FIG. 5. Absorption resonance linewidths, measured values, and fitted linear frequency dispersions (dashed lines) for the edge modes (open triangles) and center modes (open squares), respectively. Open circles in (b) and (c) denote mixed modes. (a)–(c) Data for different lattice symmetries and bias-field orientations, as indicated in the insets.

found in the amplitude maps for applied fields $H_0 < 60$ mT. Figures 4(a) and 4(b) show that for $\mu_0 H_0 = 20$ mT, the oscillation mode features two amplitude maxima for H_0 in the $[1\bar{2}]$ orientation and one amplitude maximum only for H_0 in the $[\bar{1}0]$ orientation.

We have also investigated the damping of the oscillation modes for the different array symmetries and applied field orientations, shown in Fig. 5. The linewidth of the peaks in the FMR data is related to the damping α by

$$\mu_0 \Delta H_{\mathrm{HWHM}}(f) = \mu_0 \Delta H^0_{\mathrm{HWHM}} + \frac{2\pi}{\gamma} \alpha f. \qquad (5)$$

The quantity $\Delta H^0_{\mathrm{HWHM}}$ is the linewidth at zero frequency and is related to inhomogeneous broadening [8]. It has been previously concluded that edge modes exhibit increased linewidth ΔH_0, as these modes are sensitive to edge imperfections from the lithography and lift-off processes [8,14].

The damping α is proportional to the slope of the linewidth plotted as a function of frequency and can be found from Eq. (5) as

$$\alpha = \frac{\gamma \mu_0}{2\pi} \frac{\partial}{\partial f} \Delta H_{\mathrm{HWHM}}. \qquad (6)$$

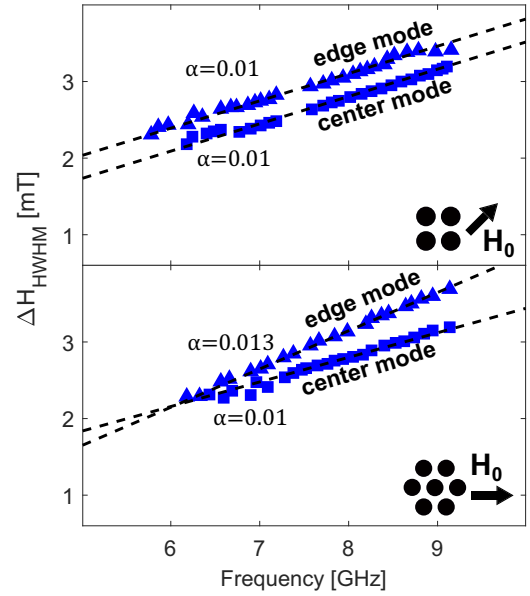

FIG. 6. Simulated absorption resonance linewidths for the edge modes (triangles) and center modes (squares). Upper panel: square array with the bias field oriented in the [11] direction, lower panel: hexagonal array with the bias field oriented in the $[1\bar{2}]$ direction.

We measure a linewidth frequency dependence with a splitting into two branches at some frequency (field) for all dipolar-coupled configurations except the square array with the applied field oriented in the [10] direction, cf. Fig. 5. In Fig. 5(a), we note that the resonance linewidth for the single disk increases monotonically with frequency in a manner similar to that observed for the square array with H_0 oriented in the [10] direction. Fitting of Eq. (6) to the frequency dispersion of the measured linewidths results in a damping constant of $\alpha = 0.006 \pm 0.001$, slightly less than that obtained for a blanket thin film of Py [8]. As center modes typically display low damping, this low value of α corroborates the result from simulations that we only excite center modes in the geometries shown in Fig. 5(a).

When H_0 is oriented in the [11] direction of the square lattice, we observe a significantly different damping behavior [cf. Fig. 5(b)]. The linewidth frequency dispersion then splits into two branches at a frequency of ~ 6 GHz. The lower branch has a modest slope, corresponding to $\alpha = 0.006 \pm 0.002$, whereas the upper branch has a steeper slope, corresponding to a damping constant $\alpha = 0.025 \pm 0.002$. We attribute this difference in damping to a different resonance mode, with the upper branch corresponding to an edge mode and the lower branch to a center mode [8]. The resonance linewidth in the low-frequency regime ($f < 6$ GHz) shown by open circles in Fig. 5(b) pertains to a mixed (edge and center) oscillation mode, as seen in simulations [cf. Fig. 3(b)].

With the hexagonal lattice [Fig. 5(c)], the difference in linewidth for the two directions of H_0 lies within the confines of the measurement uncertainty. The linewidth frequency dispersion splits into two branches at ~8 GHz, i.e., at a higher frequency than that observed for the square lattice with H_0 oriented in the [11] direction. The low-frequency part ($f < 8$ GHz) of the linewidth dispersion (open circles) again

pertains to a mixed oscillation mode (cf. Fig. 4). For $f > 8$ GHz, the center mode has a damping constant $\alpha = 0.009 \pm 0.003$, which is higher than that of the isolated disk. The damping constant of the edge mode in the hexagonal lattice is $\alpha = 0.044 \pm 0.004$, almost twice the value obtained for the square lattice. We note from scanning electron microscopy (SEM) images of the nanomagnet arrays [cf. Figs. 1(a) and 1(b)] that there is negligible difference in edge roughness between the hexagonal and the square lattice, which indicates that the difference in damping between the two arrays can be attributed to the intermagnet coupling. Micromagnetic simulations show (cf. Fig. 6) that the damping of the edge mode exceeds that of the center mode for the hexagonal lattice, while the two modes are damped equally for the square lattice with the field oriented in the [11] direction. This difference in damping indicates that the edge mode is more sensitive to the lattice symmetry, which is plausible given that the magnetic moments at the edges of neighboring nanodisks are more closely separated ($\sim$100 nm) than their centers ($\sim$400 nm). In all cases, the measured damping of the edge mode is noticeably higher than in simulations. This is most likely due to edge roughness on the fabricated nanodisks. Numerical investigations on lattices with dipolar-coupled nanospheres have been carried out previously by Mitsumata and Tomita [24], who also found that the damping is modified by dipole interactions between nanomagnets.

IV. CONCLUSIONS

Dipolar coupling between magnetic nanodisks in a lattice is found to have a profound impact on the dynamic response. This is seen from a distinct difference in the FMR spectra compared to a reference sample with uncoupled disks. Moreover, the lattice symmetry and the direction of the FMR bias field are found to promote different magnetic oscillation modes in the individual disks. The field dependence of the resonance for a square lattice with the bias field imposed in the [10] direction shows a single dominant Kittel curve across the full frequency range. A square lattice with the field imposed in the [11] direction, however, shows a Kittel curve splitting into edge- and center-mode branches for higher frequencies. Such a splitting is also observed for a hexagonal lattice, irrespective of the bias-field direction. Moreover, we observe no anisotropy in dynamic response for this lattice geometry. The lattice symmetry and the orientation of the bias field are also found to impact the effective magnetic damping, α, with highest damping for the edge mode in the hexagonal lattice. The experimental results are corroborated by micromagnetic simulations. The present findings will be of importance to the design and understanding of magnonic crystals.

ACKNOWLEDGMENTS

We would like to thank Agne Ciuciulkaite and Jonathan Leliaert for stimulating discussions. S.D.S. acknowledges support from the ALS Doctoral Fellowship in Residence. The Advanced Light Source is supported by the Director, Office of Science, Office of Basic Energy Sciences, of the US Department of Energy under Contract No. DE-AC02-05CH11231. Q.L., M.Y., and Z.Q.Q. acknowledge support from the US Department of Energy, Office of Science, Office of Basic Energy Sciences, Materials Sciences and Engineering Division under Contract No. DEAC02-05-CH11231 (van der Waals heterostructures program, KCWF16). Partial funding was obtained from the Norwegian PhD Network on Nanotechnology for Microsystems, which is sponsored by the Research Council of Norway, Division for Science, under Contract No. 221860/F60. The Research Council of Norway is acknowledged for the support to the Norwegian Micro- and Nano-Fabrication Facility, NorFab, Project No. 245963/F50.

[1] A. Chumak, A. Serga, and B. Hillebrands, J. Phys. D: Appl. Phys. **50**, 244001 (2017).
[2] M. Krawczyk and D. Grundler, J. Phys.: Condens. Matter **26**, 123202 (2014).
[3] V. V. Kruglyak, S. O. Demokritov, and D. Grundler, J. Phys. D: Appl. Phys. **43**, 264001 (2010).
[4] S. Neusser and D. Grundler, Adv. Mater. **21**, 2927 (2009).
[5] J. W. Kłos, M. Sokolovskyy, S. Mamica, and M. Krawczyk, J. Appl. Phys. **111**, 123910 (2012).
[6] E. Wahlström, F. Macià, J. E. Boschker, Å. Monsen, P. Nordblad, R. Mathieu, A. D. Kent, and T. Tybell, New J. Phys. **19**, 063002 (2017).
[7] S. Tacchi, M. Madami, G. Gubbiotti, G. Carlotti, H. Tanigawa, T. Ono, and M. P. Kostylev, Phys. Rev. B **82**, 024401 (2010).
[8] J. M. Shaw, T. J. Silva, M. L. Schneider, and R. D. McMichael, Phys. Rev. B **79**, 184404 (2009).
[9] Y. Huo, C. Zhou, L. Sun, S. T. Chui, and Y. Z. Wu, Phys. Rev. B **94**, 184421 (2016).
[10] H. T. Nembach, J. M. Shaw, T. J. Silva, W. L. Johnson, S. A. Kim, R. D. McMichael, and P. Kabos, Phys. Rev. B **83**, 094427 (2011).
[11] F. Guo, L. M. Belova, and R. D. McMichael, Phys. Rev. Lett. **110**, 017601 (2013).
[12] S. Tacchi, G. Gubbiotti, M. Madami, and G. Carlotti, J. Phys.: Condens. Matter **29**, 073001 (2016).
[13] M. Kostylev, R. Magaraggia, F. Y. Ogrin, E. Sirotkin, V. F. Mescheryakov, N. Ross, and R. L. Stamps, IEEE Trans. Magn. **44**, 2741 (2008).
[14] N. Ross, M. Kostylev, and R. L. Stamps, J. Appl. Phys. **109**, 013906 (2011).
[15] G. Woltersdorf, Ph.D. thesis, Simon Fraser University, 2004.
[16] A. Vansteenkiste, J. Leliaert, M. Dvornik, M. Helsen, F. Garcia-Sanchez, and B. Van Waeyenberge, AIP Adv. **4**, 107133 (2014).
[17] V. Flovik, F. Macià, J. M. Hernàndez, R. Bručas, M. Hanson, and E. Wahlström, Phys. Rev. B **92**, 104406 (2015).
[18] R. D. McMichael and M. D. Stiles, J. Appl. Phys. **97**, 10J901 (2005).

[19] E. Montoya, T. McKinnon, A. Zamani, E. Girt, and B. Heinrich, J. Magn. Magn. Mater. **356**, 12 (2014).
[20] C. Kittel, Phys. Rev. **73**, 155 (1948).
[21] B. Kalinikos and A. Slavin, J. Phys. C: Solid State Phys. **19**, 7013 (1986).
[22] M. Grimsditch, G. K. Leaf, H. G. Kaper, D. A. Karpeev, and R. E. Camley, Phys. Rev. B **69**, 174428 (2004).
[23] P. Politi and M. G. Pini, Phys. Rev. B **66**, 214414 (2002).
[24] C. Mitsumata and S. Tomita, Phys. Rev. B **84**, 174421 (2011).